Materials Technology Reports 2025, 3(1), 2325.
https://doi.org/10.59400/mtr2325

Review

A study of the underlying dynamics of phase-space projection of microwave-assisted synthesis of transition metal nanostructures

Victor J. Law*, Denis P. Dowling

School of Mechanical and Materials Engineering, University College Dublin, Belfield, Dublin, Ireland
*** Corresponding author:** Victor J. Law, viclaw66@gmail.com

CITATION

Law VJ, Dowling DP. A study of the underlying dynamics of phase-space projection of microwave-assisted synthesis of transition metal nanostructures. Materials Technology Reports. 2025; 3(1): 2325. https://doi.org/10.59400/mtr2325

ARTICLE INFO

Received: 18 November 2024
Accepted: 26 December 2024
Available online: 2 January 2025

Abstract: The study brings together in a single publication the phase-space projection analysis of microwave-assisted synthesis of transition monometallic (palladium, silver, platinum, and gold), binary zinc oxide, and metals supported on carbon framework nanostructures. It is shown for a database of fifty microwave-assisted syntheses, a two-variable power-law signature (y = cxn) over four orders of magnitude. The purpose of this study is therefore to identify the underlying dynamics of the power-law signature. A dual allometry test is used to discriminate between transition metal period and row, and between recommended Green Chemistry, problematic Green Chemistry, and non-Green Chemistry hazardous solvents. Typically, recommended Green Chemistry exhibits a broad y-axis distribution within an upper exponent = 1 and lower exponent = 0.5. Problematic Green Chemistry exhibits a y-axes narrower distribution with an upper exponent = 0.94 and a lower exponent = 0.64. Non-Green Chemistry hazardous data shows a further narrowing of the y-axis distribution within upper exponent = 0.87 and lower exponent = 0.66. Mass-based environmental factor is used to calculate the 'Greenness' of single-step (facile) transition metal synthesis. The power-law signature also exhibits phase transitions associated with microwave applicator type.

Keywords: microwave-assisted synthesis; transition metal nanostructures; power-law signature; allometry scaling; green chemistry

1. Introduction

In this post-COVID-19 pandemic world, the approach to health care has changed in the short term, and most likely in the long term due to social politics, Earth's resources, and energy consumption. This upheaval is leading to new forms of sustainable antibacterial, antiviral, anticancer and medicines and biotherapy [1]. These changes were already foreseen by Anastas [2] who further incorporated twelve principles into the concept of Green Chemistry; where the design of a chemical product eliminates the generation of waste through efficiency at the atom and energy level [3], and Bharadwaj et al. [4]. Recently energy phase-space projection analysis of historical non-thermal microwave-assisted inactivation of microorganisms [5] and microwave-assisted synthesis of Gold (Au) and silver (Ag) nanostructures [6] have been performed. Further to these metals, zinc (Zn), palladium (Pd) and platinum (Pt) were investigated [7]. This body of work developed a discrimination power-law test between transition metal precursors, and between recommended Green Chemistry and non-Green Chemistry [8]. The power-law test fulfils the criteria of Andriani and McKelvey [9], Stumpf and Porter [10], and Roman and Bertolotti [11] where four orders of magnitude provide a high degree of confidence in the verification of a scale-free power-law signature. More recently Hınıs et al. [12] have used such energy analysis to show that microwave-assisted synthesis of Ag nanoparticles is more rapid,

effective, and energy-efficient when compared to traditional (thermal) methods.

2. Aims of this work

This work reviews, updates, and reinterpret the information presented in [5–8] into one single comprehensive publication that describes the energy efficiency within chemistry space for transition metals nanostructures in the form of: monometallic, bimetallic, binary metal oxide and metal supported of carbon framework. What makes a chemical or energy mechanism 'Green' is it use in a given context. The term 'Green' comes from the chemical's ability to reduce the amount of material used, reduction in synthesis energy, and the reduction in the generation of unrecoverable waste. In the early developmental days of Green Chemistry there was no built-in economic component, this shortcoming was soon realized in sustainable chemistry with 'greener' or 'eco-friendly' products implicitly marketed with a social and human health impact [13]. This work uses the following definition for microwave-assisted synthesis Green Chemistry:

'*Green Chemistry encompasses the linear energy and chemical flow, within the microwave-assisted synthesis of the target product and its waste*'

Thus, the vague 'sustainable' and 'eco' adjectives now become redundant when a single-step chemical transformation (i.e., metal precursor + reactants → product + waste) is considered. However, the chemical make-up of a nanostructure product that is designed to kill a targeted organism may also be toxic to other organisms in the wider environment [14].

The remainder of this work is divided into the following sections. Section 3 provides an overview of Microwave-assisted synthesis of Zn, Pd, Ag, Pt, and Au nanostructures of transition metals. Section 4 considers microwave-assisted synthesis mass-based Environmental-Factor (E-Factor) metrics, or greenness indictor, for solid spherical or oval-like nanostructures. The E-Factor calculation (waste g/product g) only includes the materials used within the microwave-assisted synthesis, therefore equivalent a simplest E-Factor (sEF) which is ideally close to zero. However, microwave-assisted synthesis of nanostructures may be a mixture of thermal and microwave steps. For this reason, sEF is replaced with the notation E-F_m, where the subscript denotes the microwave step. Section 5 describes experimental data collection and construction of the high-dimensional space [15] called Database B. Section 6 explores the energy phase-space projection of Database B, where the process energy budget (cavity-magnetron power multiplied by process time ($J{\cdot}s^{-1}$ multiplied by s = kJ) is plotted on the *x*-axes and the process energy density (process energy budget divided by suspension). It is shown that a zero-dimension (0-D) model of Database B, yields a global two-variable power-law signature over four orders of magnitude in both *x*-axes and *y*-axes is obtained in Equation (1).

$$y = cx^n \tag{1}$$

where: y is the energy density, x is the energy value on the *x*-axes, c is the *y*-axes intercept constant, and n is the exponent of the power-law. When $n < 1$ this relates to a slow rate of energy density; an exponent = 1 means the relationship is linear; and for $n > 1$ the rate energy density is rapid, indicating a form of positive feedback

mechanism between input and outputs. As with Andresen et al. [16] we ask the question: 'Does the empirical scaling law provide functional information?' To explore these questions section 6, uses allometry [17,18] to discriminate the chemical and microwave-assisted aspects of the power-law signature. Here a dual allometry approached is used as the discrimination test with regard to the third principle of Green Chemistry, where flammable and toxic regents and organic-metals (bromine (Br), potassium (K), and sodium (Na)) should be replaced with compounds that are benign to the environment. Or as in the case of the seventh principle the use of natural plant-based biomass extract is the choice of use. Section 5 provides a ranked residual error analysis of the 0-D model. Section 7 presents and extends allometry scaling of microwave-assisted synthesis Database B. And finally, Section 8 summarizes this work, and section 9 provides an outlook.

3. Microwave-assisted synthesis of Zn, Pd, Ag, Pt, and Au nanostructures

Microwave-assisted synthesis of transition metal nanostructures requires a metal precursor, a reducing agent to release the metal seed, and a surfactant [19], all mixed in a solvent that is illuminated with microwave energy to produce the nanostructure and waste product. The E-F_m is calculated as the mass of the waste product divided by the mass of the final product (waste g/product g) which ideally should be close to zero to reflect the 'Greenness' of the synthesis [13]. This section provides a commentary on some aspects of the synthesis.

3.1. Zn, Pd, Ag, Pt, and Au transition metal chemistry

It is well known that transition metals form ionic-to-covalent bonding with other elements, where the bonding mechanism is dependent on the metal oxidation state. Where a low oxidation state produces ionic bonding, and high oxidation states produce covalent compounds or polyatomic ions. While the name *transition* has no particular chemical meaning, these elements, or metals, occupy columns in the middle of the modern periodic table, Group 2A and Group 3A. They are also sometimes called *d*-block elements, since in this region the *d*-orbitals are being filled in [20]. The most non-reactive of these metals (Au) having been mined for thousands of years, followed closely by Zn [21]. In the 16th century the scarce precious metal Pt was discovered by Europeans in Central America and much later in 1803 Pd was found. Traditionally in their bulk form these metals are used in jewelry, glassware, coinage, as a metal protection layer (galvanized steel), antifouling paints, toothpaste, and skin care products.

Today, transition metal nanostructures are produced for their unique properties. Silver has little known purpose within living cells yet monometallic Ag and Ag decorated nanostructures are fabricated for their biocide activity against targeted gram-negative, gram-positive bacteria and for air purification at environmental temperatures (20 ℃–25 ℃). The transition metal Zn is one the trace elements that is essential for biological processes in almost all living cells; in its binary oxide form ZnO is used across a range of electrical, biomedicine and cancer therapeutic applications. Whereas Pd, Pt and Au nanostructures are stable with low toxicity that

enable them to have their surface chemical composition altered (functionalized) with drug biomolecule payloads.

Figure 1 shows the relative *d*-block position and atomic number for Zn, Pd, Ag, Pt, and Au within the modern Periodic Table. In this representation, the noble gas shorthand, shows that Zn is positioned at the end of the first transition period and row with an electron configuration of [Ar] $4s^2$ $3d^{10}$: Pd and Ag are in the second transition period and row with electron configurations of [Kr] $4d^{10}$ $5s^0$ and [Kr] $4d^{10}5s^1$, respectively: and finally Pt and Au are positioned on the third period and row with an electron configurations of [Xe] $4f^{14}$ $5d^9$ $5s^1$ and [Xe] $4f^{14}$ $5d^{10}$ $5s^1$, respectively. In all cases the *d*-orbital filling increases from left to right and the electron core increases with period and row number. Both of which reduce the effective nuclear charge on the outer electrons due to electron core shielding effect, which in turn influences the atomic and chemical properties of the metal.

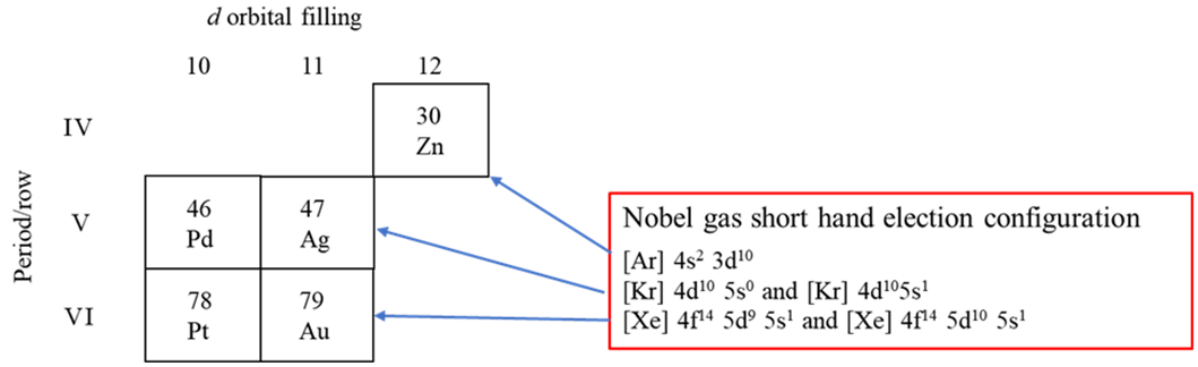

Figure 1. *d*-block transition metals (Zn, Pd, Ag, Pt, and Au) relative position within the modern periodic table according to their period and row and *d*-orbital electron filling. Also shown is their electron configuration.

In the case of Zn, *d*-orbital filling is at a maximum with ten electrons that are paired, which leaves the two outer most valence electrons almost exclusively available to participate in ionic bonding with other elements. For instance, $ZnCl_2$ or ZnO, where Zn is said to have an oxidation state +2. For this reason, Zn is sometimes considered not to be a transition metal. In the first transition metal period and row, Zinc acetate dihydrate ($Zn(CH_3CO_2)_2{\cdot}2H_2O$: molar mass 219.53 $g{\cdot}mol^{-1}$ with 57.9% Zn by weight) is employed as the metal precursor in [22–32] and therefore shall be discussed further in this work. For the second transition metal period and row, Pd tends to keep its ten electrons as 5-electron pairs to maintain a full *d*-orbital configuration, whereas Ag tends to give up its unpaired electron in the form of a surface layer of Ag_2S, or tarnish. For Pd precursors: palladium(II) acetylacetonate ($Pd(C_5H_7O_2)_2$: molar mass 304.64 $g{\cdot}mol^{-1}$) palladium(II) chloride ($PdCl_2$), palladium(II) nitrate ($Pd(NO_3)_2$) are typically used [33–35]. In each case the palladium metal as an oxidation state of +2, where two of the *d*-orbital electrons are used. For the silver precursor, silver nitrate ($Ag(NO_3)$), where Ag has an oxidation state of +1 is invariably used [12,36–47]. For the third period and row metals, Au tends to give up its unpaired electron, whereas Pt tends to keep the unpaired electron due to the attraction force of the incomplete ($5d^9$) *d*-orbital. For microwave-assisted synthesis of these transition metal nanostructures: Typically hexachloroplatinate(IV) acid ($H_2PtCl_6{\cdot}xH_2O$) is used for the Pt metal precursor [48–

51], where Pt has an oxidation state of +4. In the case of Au, tetrachloroauroic(III) acid ($HAuCl_4 \cdot xH_2O$; molar mass 339.785 $g \cdot mol^{-1}$) with an Au oxidation state of +3 is normally used [37,52–61]. For this precursor, 100 ml of 1% solution contains 1 gram of Au.

Today monometallic, bimetallic, and metal supported on carbon framework nanostructures have at least one dimension <100 nm. Their comparative size to cellular components also enables effective medical therapy, and drug delivery systems to be manufactured for the killing of coronavirus [62].

When represented as a thermodynamically stable unit cell: Pd, Ag, Pt and Au have a face-centered cubic (FCC) crystal lattice where each atom has a coordination number (the number of closest bonded neighbors) equal to 12, and the number of atoms per unit cell equal to 4 [63,64] **Figure 2**. Zinc, however, forms a more complex hexagonal close-packed (HCP) or Wurtzite unit cell, where six Zn atoms form a hexagon surrounding a central Zn atom with the next plane situated halfway up the unit cell *c*-axis that contains three additional Zn atoms situated at interstices of the HCP plane (Baranov, Sokolov and Solozhenko (2022) [65]). The coordination number for HCP is the same as FCC, but the number of atoms per unit cell are reduced to six. Under ambient pressure and temperature the binary compound zinc oxide also forms a HCP wortzite lattice (*w*-ZnO) crystal structure that exhibits an anisotropic ionic characteristic due to the O atoms that form alternating layers in the *c*-axes. This ionic characteristic is revealed in its four characteristic crystal surfaces: two *c*-axes orientated with either a (0001) polar Zn-termination or a polar (1001) polar O-termination, and two different non-polar surfaces in the *a*-axes $[11\bar{2}0]$ and *a*-axes$[10\bar{1}0]$ direction.

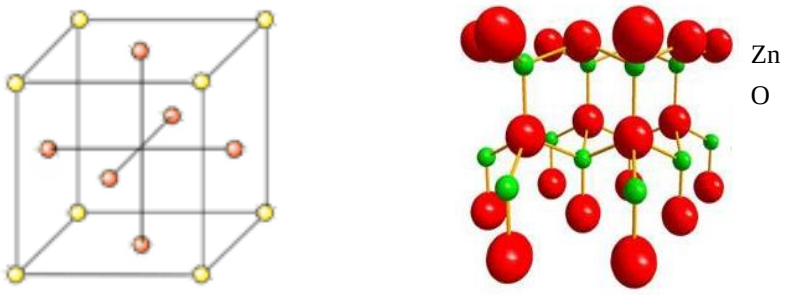

Figure 2. FCC unit cell lattice structure of Pd, Ag, Pt and Au (left) and ZnO wurtzite unit cell (right).

3.2. Transition metal precursor reduction steps

In this section three representative microwave-assisted syntheses are explored, one from each transition metal period or row. Here stoichiomertic representative balanced equations for ZnO, Pd and Au nanostructures synthesis are presented where the seed particle is denoted with a superscript 0 and typically 1.5 nm. As regard to reported colloidal suspension temperature, the accepted view is that within the microwave illumination period, polar molecules undergo dipole polarization and when these dipoles try to align with the electromagnetic field they generate heat that causes

an instantaneous temperature (T_i) causing the local non-polar compounds to be heated. For the metal precursors a second mechanism that involves currents of free charges excited at the surface and within contributes to heating because of Ohmic loss. The key advantage of microwave processing over thermal processes is the speed of the microwave reaction and the increase or decrease in temperature of the reaction. This leads to an increase in the yield of the target product molecule and corresponding reduction in side-chain reactions. It is this dual heating characteristic that makes microwave processing 'Green' when compared to traditional thermal processing. For the colloidal suspension reported they have, in general, a reported bulk temperature (T_B) that is much lower than T_i. In this work the reported colloidal solution in each referenced paper the temperature is given in degree centigrade (℃).

For the first transition period and row, the work of Wojnarowicz et al. [28], Wojnarowicz et al. [29] illustrates the contrasting dielectric properties of H_2O and ethylene glycol ($C_2H_4(OH)_2$) under different temperature and pressure conditions influence both the morphology and Co doping of ZnO nanostructures. These reactions are performed in the ERTEC microwave applicator under solvothermal conditions, where initially 2.18 g of $Zn(CH_3COO)_2{\cdot}H_2O$ is soluble in 100 ml of $C_2H_4(OH)_2$ at room temperature [66]. The representative balanced microwave-assisted solvothermal synthesis equation for these reactions are given Equation (2) (morphology), and Equation (3) (Co doping).

$$(CH_3CO_2)_2Zn{\cdot}2H_2O \xrightarrow{C_2H_4(OH)_2,H_2O,220^oC} ZnO + waste\ products \quad (2)$$

where ZnO represents the general nanostructure at $T_B \sim 220$ ℃ (means of temperature measurement not given) and an autogeneous pressure of 5 bar. As the total H_2O contents increases from 1 to 4% by weight within the reactants a change in morphology is induced from spheroid to hexagon, as the ZnO(s) grows in size.

$$(CH_3CO_2)_2Zn{\cdot}2H_2O + (CH_3CO_2)_2Co{\cdot}2H_2O \xrightarrow{C_2H_4(OH)_2,\ H_2O,190^oC} Zn_{1-x}Co_xO + waste\ products \quad (3)$$

where $ZnO_{1-x}Co_xO$ represents the general nanostructure at $T_B \sim 190$ ℃ (means of temperature measurement not given) and an autogeneous pressure of 5 bar. The total H_2O contents control the size of the nanostructure typically less than 1.5% by weight yields a particle size below 28 nm, and 5% by weight yield particle sizes above 53 nm. The crystal characterization indicates that structure is in HCP wortzite phase.

The microwave-assisted hydrothermal synthesis of Ag decorated ZnO nanostructure via the reduction of $Zn(CH_3COO)_2{\cdot}H_2O$ in a mixture of $AgNO_3$ and $C_2H_4(OH)_2$ [30] suggests the following possible representative balanced reaction Equation (4). Where the reaction is performed in an atmospheric pressure reflux apparatus within a microwave oven with the colloid solution temperature maintained at $T_B \sim 200$ ℃ (means of temperature measurement not given). The $C_2H_4(OH)_2$ and caustic sodium peroxide (Na_2O_2) act as the metal precursor reducing agents. The AgZnO represents the Ag decorated ZnO flower-like nanostructures with the Ag component having a FCC crystal lattice structure and ZnO component having a HCP wortzite crystal lattice structure.

$$(CH_3CO_2)_2Zn{\cdot}2H_2O + AgNO_3 \xrightarrow{C_2H_4(OH)_2,\ H_2O,Na_2O_2 \sim reflux,200^oC} AgZnO + waste\ products \quad (4)$$

For the second transition period and row the microwave-assisted synthesis of Pd supported on a carbon triazine framework (CTF) is given. The CTF having a high surface area with high porosity and abundance nitrogen nanostructure is synthesized is performed within the CEM-Corporation Discover® (henceforth called Discover®) applicator operating in the batch mode (here called for the following process conditions: microwave power = 100 W for 20 min that result in a T_B ~ 200 °C [35].

$$Pd(C_5H_7O_2)_2 + PCD \xrightarrow{[BMIm][NTf_2],250^oC} Pd - CTF + waste\ products \quad (5)$$

Here the metal precursor $Pd(C_5H_7O_2)_2$ is mixed with 2, 6-dicyanopyridine (PCD, $C_5H_7N_3$), which is dispersed in the solvent 1-butyl-3-methylimidazolium bis(trifluoromethylsulfonyl)imide ($C_{10}H_{18}F_6N_3O_4S_2$, or [BMIm][NTf_2]). The solvent is in the family of room-temperature ionic liquid (IL) is a charged fluid that contains both Cations and Anions of different sizes and shapes, and where their intrinsic ionic conductivity provides it with high microwave absorption properties, or high loss tangent, $tan\ \delta_e = \varepsilon_r''/\varepsilon_r'$, which is a measure of the conversion of microwave into thermal energy, Yang et al. [67], and Kustov and Vikanova [68]. The shorthand name [BMIm][NTf_2]) for this IL is used here as the Brackets usefully denote the Cation and Anion. Upon microwave illumination both dipole polarization and ionic conduction (oscillation of the ions within the electromagnetic field) occur, and where metal nanostructures are present eddy currents are induced in the metal resulting in heating due to Ohmic losses [68,69]. The combined effect is to induce an enhanced instantaneous temperature (T_i) than dipole polarization along. The outcome of this synergistic heating is to enhance rapid heating resulting in a chemical transformation at lower T_B.

For the third period and row the microwave-assisted synthesis of Au is exemplified. Here Equation (6) provides the first stage of the synthesis of Au^0 via the chemical reduction of $HAuCl_4$ with the reduction and stabilizing agent anhydrous trisodium citrate ($Na_3C_6H_5O_7$) typically diluted at 0.57 mg per 1 ml of H_2O.

$$HAuCl_4.4H_2O + Na_3C_6H_5O_7 + 18H_2O \rightarrow Au^0 + H^+ + 3Na^+ + 4Cl^- + 21H_2O + C_6H_5O_7.H_2O \quad (6)$$

$$Au^0 \xrightarrow{Na_3C_6H_5O_7} AuNP \quad (7)$$

The growth of the Au nanostructures from Au^0 seed is given in Equation (7) where the size of the Au nanostructures depends strongly on the ratio of $Na_3C_6H_5O_7$ to $AuCl_4$. This is because $Na_3C_6H_5O_7$ also acts as a stabilization agent. A typical scenario for this dual process is generally expressed by the following example. At low $Na_3C_6H_5O_7$ concentrations, the growing Au^0 seed particle has a low probability due to low chance of reaction with a $Na_3C_6H_5O_7$ molecule; consequently aggregation occurs resulting in an increase in Au particle size and size distribution, both of which are accompanied by a variety of particle morphologies. At large $Na_3C_6H_5O_7$ concentrations, the Au^0 seed has a high probability of reacting with a $Na_3C_6H_5O_7$ molecule and is rapidly stabilized with a small spherical diameter and size distribution. In many respects, the critical difference in $Na_3C_6H_5O_7$ concentration is a mass transport phenomenon where the supply of $Na_3C_6H_5O_7$ defines the position of the rate-limiting step of Au nanostructure growth. Naturally, particle growth stops when all the $HAuCl_4$ is consumed in the reaction. For Ag nanostructure synthesis, the Au precursor

is normally replaced with silver nitrate ($AgNO_3$) in the presence of a reducing reagent.

3.3. Surfactants

Surfactants molecules have a hydrophilic head and a long hydrophobic tail. Polyethylene glycol is a typical example of this amphiphilic trait and plays an important role in the formation of transition metal nanostructures [25] and Kawasaki et al. [70]. Where microwave illumination conditions produce colloidal temperature close or above the boiling point of $C_2H_4(OH)_2$ (197 ℃ at one atmospheric pressure), $C_2H_4(OH)_2$ acts as both a reducing reagent, and also absorbs on the (0001) ZnO polar surface to restrict ZnO crystal growth along the [001] direction, in doing so promoting nano-sheet structures and flower-like growth [30]. The surfactant process is thought to proceed by a two step oxidation of $C_2H_4(OH)_2$ to produce glycololdehyde ($C_2H_4O_2$) that has a terminating oxygen and hydride at either end of its very short carbon chain.

3.4. Microwave (2.45GHz) dielectric properties H_2O and $C_2H_4(OH)_2$

The reactions **Equation 5** involve [BMIm][NTF_2] has very different dielectric properties to that of H_2O and $C_2H_4(OH)_2$ at environmental temperatures of 20–25 ℃ therefore has different microwave absorbing properties. Molecular H_2O is classed as a moderate microwave energy absorber with a *tan* δ_e of approximately 0.16 at 20 ℃. Whereas [BMIm][NTF_2] and $C_2H_4(OH)_2$ at environmental temperature are classed as fast microwave energy absorbers with a *tan* δ_e of approximately 0.56 [67], and 1.35 [71,72]. The dielectric properties (real (ε_r') and imaginary (ε_r'')) parts of its complex permittivity, and *tan* δ_e are given in **Table 1** for 20 to 25 ℃ and at a temperature of 100 ℃ [73]. This comparison shows the that $C_2H_4(OH)_2$ with its boiling point (197 ℃) at atmospheric pressure and high *tan* δ_e will be more effective in absorbing microwave energy, consequently will be rapidly heated at higher temperatures compared to H_2O. For this reason, distilled H_2O is the primary solvent used in the microwave hydrothermal synthesis of ZnO nanostructure and is replaced by $C_2H_4(OH)_2$ in the solvothermal synthesis of ZnO nanostructures. Although at present there is no high temperature data for [BMIm][NTF_2], it is expected to have similar properties to that of $C_2H_4(OH)_2$.

Table 1. Distilled H_2O and $C_2H_4(OH)_2$ real and imaginary complex permittivity, *tan* δ_e at 2.45 GHz for 20 to 25 ℃ and 100 ℃ at one atmospheric pressure.

Solvent	**Boiling point (℃)**	ε_r' **(20 to 25 ℃)**	ε_r'' **(20 to 25 ℃)**	*tan* δ_e $\varepsilon_r''/\varepsilon_r'$	ε_r' **(100 ℃)**	ε_r'' **(100 ℃)**	*tan* δ_e $(\varepsilon_r''/\varepsilon_r')$
H_2O (distilled)	100	~78	~12.5	~0.16	~80.4	~9.889	~ 0.045
[BMIm][NTf_2]	< 100	~6.2	~3.5	~0.56	-	-	-
$C_2H_4(OH)_2$	197	~37	~49.95	~1.35	~25	~4	~0.16

4. Microwave-assisted synthesis E-F_m

This section presents mass-based E-F_m metrics, or 'Greenness' indicator of microwave-assisted synthesis of ZnO spheres [28], Pd spheres supported on a carbon framework [35] and monometallic Ag [38] and Au [57] nanostructures. In each case the synthesis employs a one-step (facile) process with the target nanostructure being a

solid spherical or oval-like in shape, this approach reduces surface area, and reactivity effects, as flower-like structures have acute angled spikes that generate large surface-to-volume ratios compared to a solid sphere, and therefore are excluded from this comparison. For the solvothermal synthesis of ZnO Equation (2) and the quantity data [28] are used. For microwave-assisted synthesis Au Equations (5) and (6) along with their quantities [57] are used. Generally, nanostructure product purification is performed by either centrifugation or a solvent post-wash, where the auxiliary materials provide an additional E-Factor calculation that goes to form a complete Environmental-Factor. For comparison purposes only, the post-wash calculation is given in *italics* for ZnO and Pd@CTF [35]. As ZnO yields of 31 to 37% have been reported by Cai and Hung (2023) [32], 50 to 88% for Pd-CTF reported by Rademacher et al. [35], and approximately Au 50% yield reported by Putri et al. [60]; a metal composition yield of 50% per metal precursor molar mass is assumed in all E-F_m calculations.

Even though the four E-F_m calculations presented in **Table 2** are limited in scope, the magnitude of their values is generally in line with the 1992 published E-Factor for the pharmaceutical industry [13]. On closer inspection the 50% metal yield E-F_m does not increase with Group period and row but rather with the stoichiometry of the nanostructure. For instance, the lowest E-F_m value is the [BMIm][NTF_2] liquid ionic solvent synthesis with a value of 21 to 25 depending on the amount of carbon framework that the Pd is decorating. This is followed by $C_2H_4(OH)_2$ synthesis which equates to an E-F_m of approximately 20.7. The third highest E-F_m value is 109 for the $HAuCl_4$ synthesis of Au. Finally, the plant-based biomass synthesis of Ag that has the highest H_2O solvent usage has an approximate E-F_m value of 116. Two features of note for these outcomes are that the post-wash step increases the value E-F_m, and in the case of the Pd supported on carbon framework synthesis is that the reducing reagent appears in the denominator of the E-F_m calculation as it becomes part of the target product [13]. Welton [74], along with others, has pointed out the limitations of this calculation in that it does not discriminate between: addition, isomerization reaction, substitution, and elimination reactions. Thus, for a final monometallic nanostructure product where all other mass is classed as waste, the amount of solvent greatly increases the E-F_m value, as in the case of plant-based biomass synthesis.

Table 2. Estimated order of E-F_m (waste g/product g) for one-step (facile) microwave-assisted synthesis of some ZnO, Pd, Ag, and Au nanostructures.

Target transition metal	**Applicator**	**Precursor mass**	**Reducing, capping, framework mass**	**Solvent mass**	***Post-wash mass***	**EF metal yield 50%**
ZnO [28]	ERTEC	$(Zn(CH_3COO)_2{\cdot}2H_2O$ ~15.36 g	*$C_2H_4(OH)_2$ 80.3 g	**H_2O 1.6 g	*H_2O* *150 g*	~20.7 *~31*
Pd@CTF [35]	Discover®	$Pd(C_5H_7O_2)_2$ ~0.0572 g	$C_5H_7N_3$ 0.020 g	[BMIm][NTf_2] 2 g	*CH_3CN* *3.144 g*	~21 to 25 *530 to 570*
Ag [38]	MO IFBl 30SC3	$AgNO_3$ 0.17 g	Osmium leaf extract 10 g	H_2O ~50 g	Not given	~1116
Au [57]	Discover®	$HAuCl_4$ 1.698 g	0.25 mM $Na_3C_6H_5O_7$	H_2O ~39.8	Not given	~109

*[66]. **Approximately 1.5% H_2O in $C_2H_4(OH)_2$. *** Three aliquots of 50 ml of H_2O.

5. Experimental data collection and high-dimensional space design

Microwave dielectric volume heating for the synthesis of organic polar and non-polar compounds is one heating technology of choice for Green Chemistry [5–8,12,34,35,36,38,46,50,53-56,59,68,72,73,75]. This is because the process induces a rapid rise in internal temperature that results in short process times and high yields as compared to thermal heat processes.

Collating experimental data from different research sources where the electrical-chemical conditions vary and are not reported uniformly invariably results in the electrical-chemical database not being complete [6–8]. Database A is collated from the electrical-chemical microwave-assisted synthesis of Au and Ag nanostructures publications [8], then updated with the electrical-chemical synthesis data of Zn, Pd and Pt to produce Database B [6]. The database generates 50 synthesis high-dimensional datasets from thirty-five papers about microwave-assisted nanostructure synthesis [22–27,29–61]. During this data-gathering process a further ten microwave-assisted synthesis of nanostructure papers [76–86] were found to have insufficient electrical-chemical data to allow full calculations, and therefore are not included in this work.

In Database B, the majority of the syntheses are performed in a domestic microwave oven, with forty-nine processes operating in the batch mode and one operating in the continuous-flow mode. In all cases, a free-running cavity magnetron operating at a frequency of f_o = 2.45 ± 0.05 GHz is used to illuminate the samples. Five of the microwave oven (Bluesky, model BMG20-8) data points represent non-thermal microwave-assisted dielectric heating of 10 ml H_2O pseudo-suspension using 55%, duty cycle (440 W of 800 W) and simultaneously cooled by an ice or ice slurry. The experiments were designed to mimic bacteriophage and *E. coli* ≥4 $\log_{10}$ inactivation [5]. This data is used as a benchmark as H_2O is considered to be a universal solvent. The remaining microwave applicators are: The Discover® applicator, the ERTEC, model 02-02 applicator operating in the solvothermal mode, temperature-controlled microwave chemistry (TCMC) applicators that typically uses a atmospheric pressure reflux apparatus; Digestion applicators that use a sealed reaction vessel operating in the solvothermal or hydrothermal mode.

Table 3. Short form of green chemistry solvents and reagents [8].

Recommended	Recommended or problematic	Problematic	Problematic or Hazardous	Hazardous	Highly hazardous
Green Chemistry		Problematic Green Chemistry		Non-Green Chemistry hazardous	
Water					
Acetic acid					
Bacterial extract					
Carboxymethyl-cellulose sodium		Potassium hydroxide			
Dextrose, Glucose Maltose and Sucrose		Sodium hydroxide		Cetyltrimethyl ammonium bromide	
Dimethyl sulfoxide		Sodium peroxide		Hydrazine hydrate	
Ethanol		(3-mercaptopropyl) trimethoxysilane			
Ethylene glycol					
Plant-based biomass extract					
Polyvinylpyrrolidone					

The electrical, chemical, and time information collated within Database B is used

to generate a high-dimensional space from which the data is dimensionally reduced for visualization as an XY scatter plot [15]. The data point color and shape are used to delineate the microwave applicator-type and metal nanostructure. A log-log transformation is used for the energy phase-space projections with a linear regression Excel power function trend-line to fit the data. This power function, generators the 0-D model that represents the process energy density prediction at each observed process energy budget value, but in itself does not give any underlying synthesis information.

Since the 1990s, the use of solvents that do not appear in the product chemical stoichiometric equation has been an environmental concern with many forms of metrics being used as an environmental selection guide [2,3,13]. Here, a shorten guide formulated from (http//www.chem21.eu/) [74] is used to provide clarity in both dataset facets and plots. The reduced guide comprises: recommended, problematic and hazardous. Using this formulation H_2O, $C_2H_4(OH)_2$, bacteria extraction and plant-based biomass extracts are in the Green Chemistry group, light molecular weight caustic chemicals compounds (potassium hydroxide (KOH), sodium hydroxide (NaOH), and Na_2O_2 are in the problematic group. Organic bromides and flammable hydrazine hydrate are in the hazardous group (**Table 3)**.

6. Energy phase-space projection of database B

Figure 3 shows the first of the energy phase-space projections for Database B: with horizontal-axes of 0.1 to 10,000 kJ, and vertical-axes of 0.01 to 1000 kJ·m^{-1}. For comparison, the non-thermal microwave-assisted data is represented by green filled circles. The Discover® applicator operating in the continuous flow for the synthesis of Au nano-rods is represented by the black-filled circle. The remaining open circles represent the digestion applicator, ERTEC, microwave oven, TCMC synthesis of ZnO, Pd, Ag, Pt and Au nanostructures. The trend line (black solid line)–represents the Microsoft least squares fit through all fifty data points.

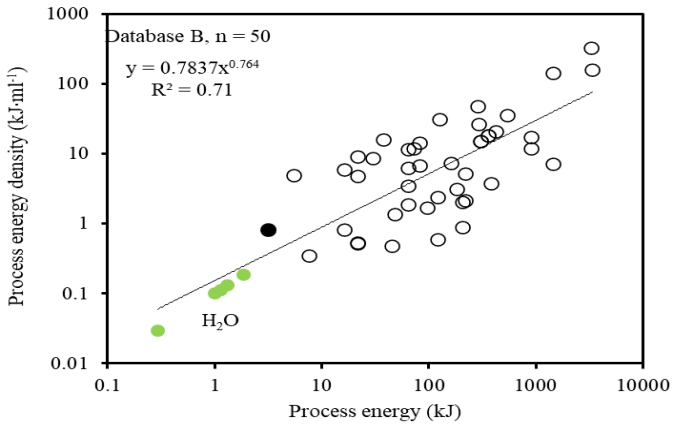

Figure 3. Log-log process energy phase-space projection of forty-four batch process microwave-assisted ZnO, Pd, Ag, Pt and Au nanostructures (open circles), one continuous flow (black filled circle), plus non-thermal inactivation of microorganisms within microwave oven (five green closed circles). Microsoft least squares fit through all fifty data points (black solid line).

The horizontal axes of this projection is related to the cavity-magnetron duty

cycle power on-time (T_{on}), where T_{on} plus T_{off} equals the base time, and T_{on} minus base-time equals to the duty cycle. Hence T_{on} is multiplied by the number of base-times used to determine the process energy budget. This accumulated time may be considered similar to mammals 'physiological-time' used in the scaling of different organism [16] and Lindstedt [87]. This means that clock-time (as seen by an outside observer) does not directly control the process energy budget. From a colloid suspension temperature point of view, T_i can be considered a constant in the accumulated time, but the T_B profile becomes desynchronized from the direction of process energy budget. Taken together with [16] the energy phase-space projection provides minimum thermodynamic entropy (H) and a maximum energy efficiency values for the solvents and reactants used in each of the individually mapped data points.

The Microsoft linear regression trend-line corresponds to a two-variable power-law function over four orders of magnitude in both x-axes and y-axes: with y-axes intercept c = 0837, and exponent n of 0.764 and R^2 = 0.6643. A number of remarks about the linear mathematical analysis may be made.

First, the variance in the data as expressed by the R^2 = 0.6643 should not be considered a poor reflection of the linear fit as there is no mathematical knowledge of the selective heating present in each data point. That is, each data point represents the outcome of the complex dipolar, ionic conduction and metal induced eddy currents occurring within the suspension subjection to microwave irradiation.

Second, the trend-line splits the data into 24 points above and 26 below with a total ± data summation = 500 kJ·ml^{-1}.

Third, the trend-line y-axes intercept is not real due to the cavity-magnetron warm-up period which approximates to 3 to 5 s [5], Law (1998) [88], and Geedipalli et al. [89]. For example, a 800 W rated cavity-magnetron operating in CW mode, the process energy budget lower limit (x_{min}) equates to 2.4 kJ.

Fourth, in log-linear space 3-Sigma mathematics can emphasis outliers that can be attributed microwave applicator-type and chemistry? Whereas in log-log space outliers that are far away from the origin are compressed resulting in the underlay chemical function is emphasis over many orders of magnitudes.

6.1. Ranked residual error analysis of database B

To access the underlying dynamic and structure of Database B, the 0-model (which take the form of the fitted trend-line) is further explored. The task here is to find data points that are far away (outliers) from the 0-model and give the outliers a specific attachment chemistry or microwave applicator-type meaning. The first step in this process is to normalize the 0-model values to zero to form an identity-line. The second step is then calculate the residual error (RE) as in Equation (8), where P_v is the 0-model predicted value and O_v is the observed experimental value.

$$RE = P_v - O_v \tag{8}$$

The RE values are the ranked in order of magnitude (from minus to positive) and plotted sequentially against the identity-line in linear space [7] and Dong [90]. The advantage of representing Database B in this way is that outliers are moved to the extremes of the identity-line sequence and their magnitude off-set from the identity-

line makes them easily identified. This method naturally highlights gross off-sets and points the researcher to further inspects the experimental data behind the outlier. This representation however tends to smooth-out small phase-transitions, thus the process is used as a data point filtering process where the degree of the outlierness is measured relative it neighbors.

Figure 4 shows the rank plot of 50 data points with the following annotation. Note how the data forms a smooth sign curve along the model identity-line, with the negative magnitudes to the left hand side and the positive magnitudes to the right hand side. The TCMC applicator group is spread out to the left, the Digestion applicator groups are spread to the right. The two ERTEC applicator data points are ranked two and thirty-one with diffidence values of −15.745 kJ.ml^{-1} for binary oxide ZnO, and +3.01 kJ.ml^{-1} for monometallic Pt. The ZnO synthesis also has an approximate E-F_m value of 20.7.

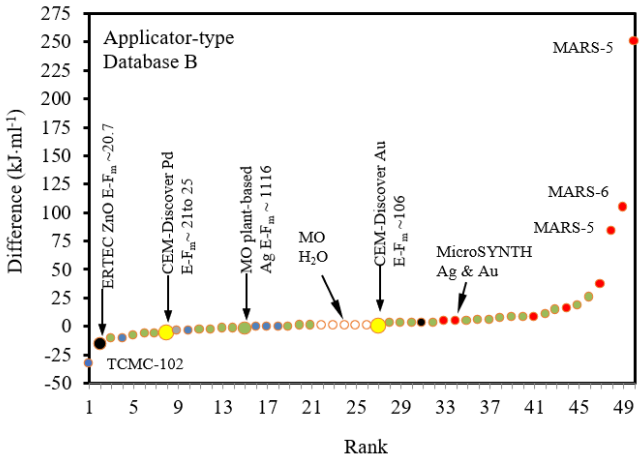

Figure 4. Database B; applicator-type ranking according to their difference from the model identity-line. Open circles (MO H_2O) represent the non-thermal microwave dielectric volume heating within a microwave oven. Blue circles TMC applicators. Black circles ERTEC applicators. Green circles microwave oven applicators. Red circle Mileston and MicroSYNTH plus Digestion applicator. Red circles represent MARS-5 and MARS-6 Digestion applicators. Large yellow circles Discover® batch and continuous flow applicators. Reproduced and updated from Law and Dowling [7].

The large yellow filled data points ranked eighth with a difference of −3.351 kJ.ml^{-1} represents the Discover® applicator operating in the batch mode for the synthesis of Pd supported on carbon framework nanostructure with an E-F_m of 21 to 25. Whereas as the large yellow filled data point ranked twenty seven with a difference of +0.436 kJ.ml^{-1} represents the Discover® applicator (operating in the continuous flow mode) synthesis of monometallic Au nanostructure with an approximate E-F_m value of 106. Between the Discover® data points, the ranked 15 data point a plant-based biomass synthesis of Ag with an approximate E-F_m value of 1116.

Note also that the MO H_2O group is positioned in the middle of the ranked data and close to model identity-line. With H_2O considered as a Green Chemistry universal polar solvent, this unique reference position, again highlights the reason why H_2O-

MO data is used as comparative reference to the transition metal nanostructure data points.

7. Allometry scaling of microwave-assisted synthesis database B

Since the pioneering of Huxley and Teissier [17,18], Kleiber [91], and Kleiber [92] the debate on the underlying mathematics of allometry scaling of heat transfer processes has been on going, and is now used in other fields of research [16,90], Gillooly [93], Downs [94], Rue [95], Agutter and Tuszynski [96], Niklas and Kutschera [97], and Lamont et al. [98]. Law and Dowling [7,8] successfully used allometry scaling for the probing the dynamics and structure of microwave-assisted synthesis Database B. In particular the use of novel non-linear dual allometry test that bracket recommend Green Chemistry within the dataset. This section presents a dual allometry Green Chemistry discrimination test with extension to group the final product into monometallic, compound metal nanostructures. Non-thermal microwave dielectrically heated H_2O is used a control comparison. The non-linear test employs an upper power function and a lower power function that brackets a portion of the dataset. The primary assumption here is that both power functions have the same y-intercept value.

7.1. Group IV ZnO

Figure 5 shows ten ZnO compound nanostructure data points are with an upper exponent = 0.9 and a lower exponent = 0.57. The first feature of note is that the original Database B trend-line (exponent = 0.7837 bisects the data points; two data points above and eight data points below, all of which are tightly grouped within 72 to 900 kJ process energy budget range.

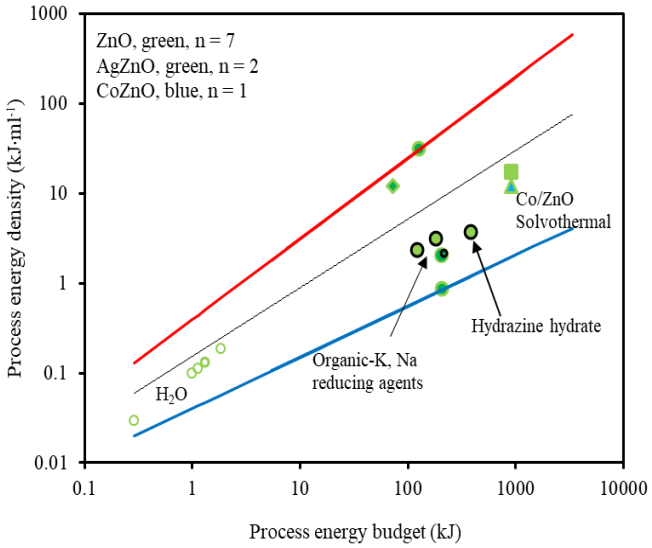

Figure 5. Log-log energy phase-space projection of seven ZnO and two AgZnO (green), and one Co doped ZnO (blue) nano-flower structures. Square = TCMC applicator, diamond = ERTEC applicator, and triangle = Digestion applicator. Green circles = Microwave oven heating of water. Allometry scaling: red line = exponent of 0.9, blue trend-line = exponent of 0.57, and thin black line = original trend-line with an exponent of 0.764. Reproduced and updated from Law and Dowling [8].

In the 0.7837 to 0.9 exponent region two microwave-assisted syntheses are located in the 72 to 126 kJ process energy budget range with an upper exponent between 0.85 to 0.9. In this group Cao et al. [22]) employed a LG-MS-2079T microwave oven for the Green Chemistry synthesis of flower-like ZnO nano-sheet aggregates (green circle). Krishnapriya et al. [27] also employed a Anton-Paar (Microwave Pro) Digester applicator for a microwave-assisted hydrothermal process (using $Zn(CH_3COO)_2{\cdot}H_2O$ + NH_3 in H_2O at a formation of ZnO jasmine-like nanostructures (green diamond).The main process parameters for this reactions was as follows: initial T_B = 50 ℃then ramped up to T_B = 125 ℃ at a autogeneous pressures up to 80 bar.

In the exponent 0.57 to 0.7837 region six microwave ovens processes are located in the 120 to 380 kJ process energy budget range. These are: Li et al. [23] used caustic NaOH to reduce $Zn(CH_3COO)_2{\cdot}H_2O$ within an unspecified microwave applicator operating at 500 W with 50% duty cycle for the synthesis of ZnO and AgZnO flower-like nanostructures (green filled circle with black ring). And Cao et al. [24] who used $C_2H_5NO_2$ and H_2O to reduce $Zn(CH_3COO)_2{\cdot}H_2O$ to form flower-like nanostructures within a Galanz microwave oven (green filled circle). Hasanpoor et al. [26] used a LG-MS1040SM microwave oven for microwave hydrothermal synthesis of ZnO flower-like structures. In their reaction toxic and farmable hydrazine hydrate is mixed with H_2O is used to reduce $Zn(CH_3COO)_2{\cdot}H_2O$, but did not report a T_B value, and whether the reaction vessel was sealed, if so no autogeneous pressure is given (green filled circle with black ring). Liu et al. [30] used a unsealed reflux apparatus to heat a mixture of $AgNO_3$ and ZnO precursors plus $C_2H_4(OH)_2$ and caustic Na_2O_2 within an unspecified microwave oven for microwave-assisted hydrothermal synthesis of bimetallic Ag and ZnO nanostructures at $T_B \sim 200$ ℃. Here it can be assumed that the reflux apparatus exit aperture was at 1 bar atmospheric pressure (green filled circle with black ring). Aljaafari et al. [31] used caustic KOH to reduce $Zn(CH_3COO)_2{\cdot}H_2O$ within an unspecified Samsung microwave oven (green filled circle with black ring). Finally, Cai and Hung [32] used a P70D10P-TE Galanz microwave oven to synthesis ZnO flower-like nanostructures (green circles). Grouped to the right at a process energy budget range of 900 kJ are two microwave syntheses. Li et al. [25] used a TCMT applicator for synthesis of ZnO flower-like nanostructures (green square), and Wojnarowicz [29] used an ERTEC microwave applicator for microwave-assisted solvothermal synthesis of bimetallic (Co doped ZnO) compact “cauliflower” nanostructures (blue triangle).

7.2. Group V: Pd and Ag

Figure 6 depicts the microwave-assisted synthesis energy phase-space for five Pd nanostructures [33–35], and fourteen Ag nanostructures [36–47]. The most striking feature of these nineteen data points is an elongated cluster over three orders of magnitude along original trend-line.

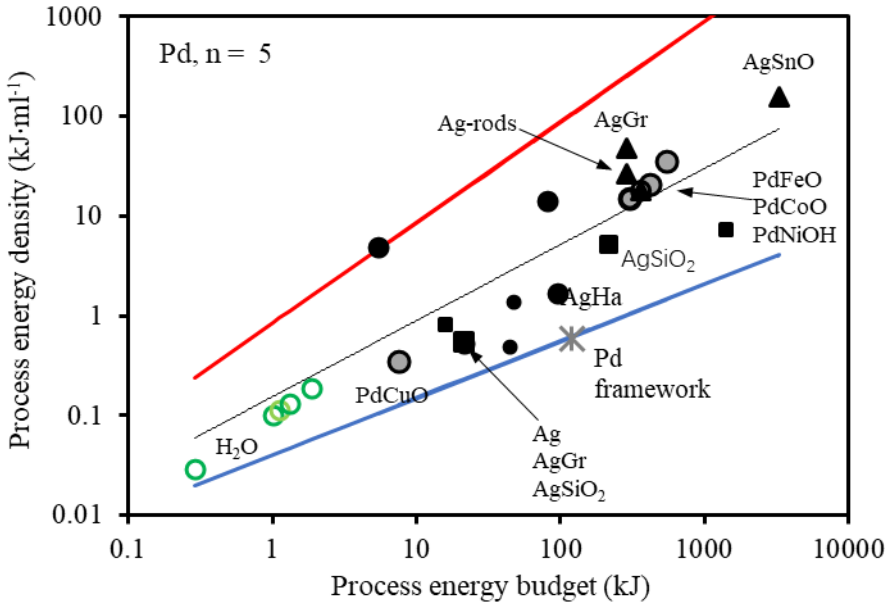

Figure 6. Log-log energy phase-space projection of five Pd (grey and star) and fourteen Ag (black) nanostructures. Star = Discover® applicator, circle = Microwave oven applicator, square = TCMC applicator, diamond = ERTEC, and triangle = Digestion applicator. Green circles = Microwave oven heating of water. Allometry scaling: red line = exponent 1.01, blue line = exponent 0.57, and black line = original trend-line with exponent = 0.764. Reproduced and updated from Law and Dowling [8].

In the case of the Pd nanostructure data, there are two applicator-types represented: an unspecified microwave oven rated with a 1 kW CW cavity-magnetron (grey filled circle) [33,34], and a Discover® applicator (star) [35]. The unspecified microwave oven employs flammable and toxic hydrazine hydrate as a reducing reagent in the synthesis of PdFe, PdCo and PdNiOH frameworks (plates) [33], and PdCuO frameworks [34]. Together their energy phase-space coordinate are closely aligned (−0.36, + 3.3, +5.5 and +17 kJ·ml^{-1}) to the original data trend-line (Large grey filled circles with black ring). Whereas the Discover® applicator employs an axial field antenna to create the electromagnetic field processing zone [35]. Here the synthesis of Pd on carbon framework nanostructures have an energy phase-space coordinate of 120 kJ and 0.6 kJ·ml^{-1} and lies at the lower boundary exponent = 0.57 (large grey star), and an approximate E-F_m value of 21 to 25. The solvent used to post-wash the Pd nanostructure has a low toxicity, thus the synthesis is positioned within the recommended Green Chemistry group.

An examination of the fourteen Ag data points reveals they are divided six above and eight below the original data trend-line, with one just above the upper exponent = 1 [40]. The latter being a one-pot microwave-assisted synthesis with $C_{20}H_{24}O_6$ acting as both a reducing and stabilizing reagent within a Samsung CE2877 domestic microwave. Here the cavity-magnetron is rated at 850 W and used at 35.3% duty cycle (300 W) for 180 seconds.

The Ag data between the original rend-line and the upper exponent = 1 comprises: one microwave oven and four Digestion applicators. For instance, Ahmed et al. [47]

uses oxalic acid ($C_2H_2O_4$) and cetyltrimethyllammoiumbromide ($C_{19}H_{42}BrN$) within a Samsung microwave oven to reduce $AgNO_3$, for the synthesis of Ag spherical nanostructures. Miglietta et al. [45]), used $C_2H_6O_2$ with an Anton-Parr Multiwave applicator for synthesis of Ag decorated graphene nanostructures. For more information on this process see Alfano et al. [99]. Liu et al. [52] employs a MARS-5 Digestion applicator for synthesis of Ag nano-rods using $Na_3C_6H_5O_7$ and Au seeds at 100 ℃. Blosi et al. [37] employs a claimed 'eco-friendly' for the synthesis AgAu core-shells using glucose ($C_6H_{12}O_6$) to reduce $HAuCl_4$ within a Milstone μSYNTH plus digestion applicator. Rai et al. [41] uses the Green Chemistry hydrothermal method for the synthesis of $Ag@SnO_2$ core–shells within a MARS-5 Digestion applicator for microwave hydrothermal process (operating temperature = 90 ℃, autogeneous pressure not reported) for the synthesis of AgSnO core-shells. Note also that the three digestion applicator synthesis are positioned to the higher end of energy phase-space (>280 kJ).

Now consider the Ag data points between the original trend-line and the lower exponent = 0.57. In this region there are three microwave ovens and five TCMC applicators synthesizing Ag nanostructures. The microwave oven syntheses are as follows: Saha, et al. [38] uses the 'eco-friendly' osmium leaf extract for the synthesis monometallic Ag nanostructures with a approximate E-F_m value of 1116. Iqbal et al. [39] used $C_{19}H_{42}BrN$ in diammonium hydrogen phosphate for substitution of Ca for Ag to form hydroxyapatite (AgHa, large black filed circle) nanostructures. Jyothi et al. [46] used *Coleus amboinicus* leaf extract synthesis of Ag nanostructures (black filled circle).

The TCMC applicators are: Chen et al. [36] employs theTCMC-102 for 'Green' syntheses of Ag nanoparticles with carboxymethyl-cellulose sodium ($C_8H_{15}NaO_8$) as the reduction and capping reagent (black filled square). Karimipour et al. [42] used a Shikoku Keisoku SMW 06 fitted with a reflux apparatus for synthesis of Ag nanoparticles (black filled square). The synthesis used dimethylformamide (C_3H_7NO) as the reducing reagent and oleylamine ($C_{18}H_{37}N$) as the capping reagent. Ebrahimi et al. [43] used the same TCMT applicator for the synthesis of AgTiOs core-shells (large black filled square). Their synthesis used ethanol as the solvent and Polyvinylpyrrolidone-40 ($(C_6H_9NO)_{40}$) as the reducing reagent. Karimipour et al. [44] also used the same TCMT applicator for synthesis of $AgSiO_2$ core-shell nanoparticles (large black filled square). In this synthesis ethanol and C_6H_9NO was used. Again from a recommended Green Chemistry claim, nine publications may be considered [37,38,40–46]. Iqbal et al. [39] and Ahmed et al. [47] used the surfactant.$C_{19}H_{42}BrN$ which in the non-Green Chemistry hazardous group.

7.3. Group VI: Pt and Au

Figure 7 depicts the microwave-assisted energy phase-space of sixteen synthesized Pt and Au nanostructures. The upper exponent = 0.95 to intercept the highest $kJ{\cdot}ml^{-1}$ data point, and the lower exponent = 0.7. Here the narrowing boundary limits indicates a reduced process energy density bandwidth as compared to the ZnO and the Pd and Ag group.

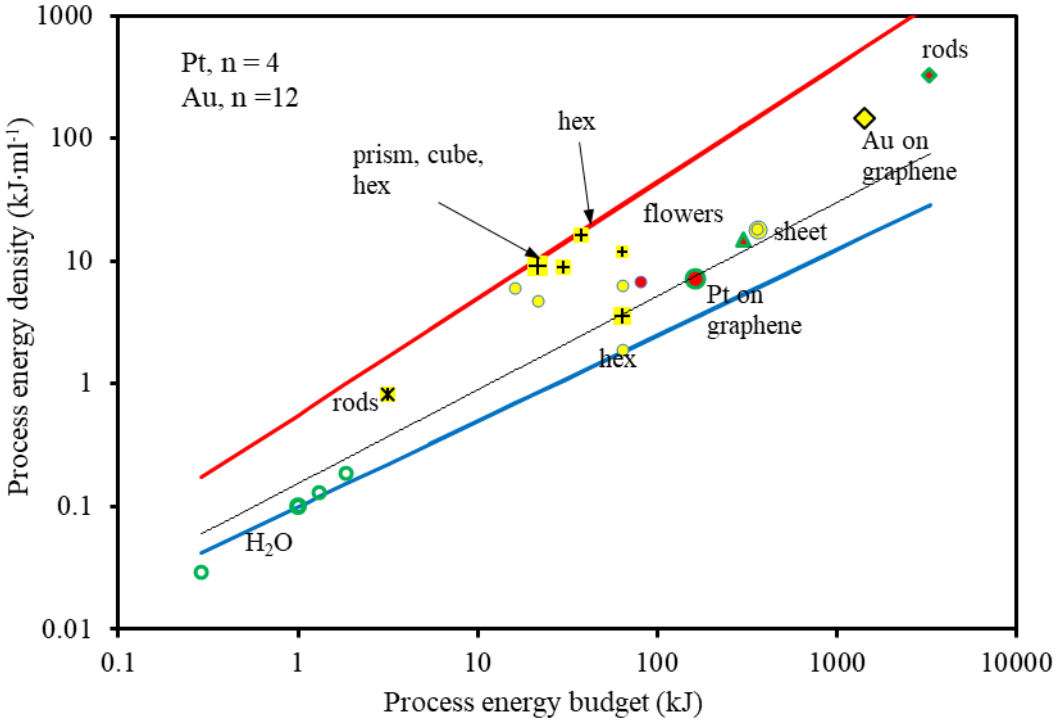

Figure 7. Log-log energy phase-space projection of four Pt (red) and twelve Au (yellow) nanostructures. Yellow star = Discover® applicator operating in the continuous-flow mode, Circle = Microwave oven, diamond = ERTEC, and triangle = Digestion applicator. Green circles = Microwave oven heating of water. Allometry scaling: red line = exponent 0.95, blue line = exponent 0.7, and black line = original trend-line with exponent = 0.764. Reproduced and updated from Law and Dowling [8].

Consider first the four Pt nanostructures data points (red filled circles, triangle and diamonds). Li et al. [48] employed a MARS-5 Digestion applicator using the solvothermal synthesis process at a temperature of T_B = 90 °C, and autogeneous pressure < 200 psi to produce nano-rods (red triangle with green ring). Kundu et al. [49] employed an unspecified microwave oven using $C_2H_4(OH)_2$ to synthesis Pt on a graphene framework nanostructures (large red filled circle with green ring). Pal et al. [50] employs a Samsung CE2877 microwave oven using a mixture $(C_6H_9NO)_n$ and $C_6H_{12}O_6$ to synthesis Pt nanostructures (red filled circle with green ring). Wojnicki et al. [51] used the ERTEC applicator working at between 25 to 225 °C and autogeneous pressure of 45 to 50 bar (red diamond with green ring). These syntheses are located close to the original Database B trend-line with values of: − 0.124, + 2.324, + 3.01 and + 25 kJ·ml^{-1}, respectively.

The twelve synthesized Au transition metal nanostructures [37,52–61] are depicted with yellow filled circles to depict spheres, and cross with yellow background to depict nanostructure other than spheres. A green outer ring indicates claimed Green Chemistry.

The lowest process energy budget reported here is Bayazit et al. [56] who used the Discover® applicator operating in the continuous-flow mode (residence time (τ) typically between 1.5, 0.85, and 0.6 min) to grow Au nano-rods (star with yellow background). In this synthesis $HAuCl_4{\cdot}4H_2O$ is reduced using $Na_3C_6H_5O_7$ diluted in distilled H_2O at an applied power of 36 W to yield a E-F_m = 106.

The cluster in the 16 to 64 kJ process energy budget range corresponds to

domestic microwave ovens used to synthesize Au nanostructures. In this cluster, Mallikarjuna and Varma [53] used an inverter circuit [100] to produce 1000 W with a 35 to 45 s illumination time within an unspecified Panasonic microwave oven using the 'eco-friendly' reactants maltose and sucrose to reduce $HAuCl_4{\cdot}4H_2O$. Yasim et al. [54] used *hibiscus rosa-sinensis* leaf extract to reduce $HAuCl_4$ within an unspecified domestic microwave oven. The cavity-magnetron conditions used where between 140, 280 and 420 W for a process time of 30, 60, and 90 s to achieve a given nanoparticle size and shape. Bhosale et al. [55] used a LG intellowave™ sensor microwave oven (model unspecified) to synthesis both spherical and flower-like nanoparticles. Their 'Greener' synthesis used the high boiling point (189 °C) lower vapor pressure (0.556 mbar) dimethyl sulfoxide (C_2H_6OS) to reduce $HAuCl_4$. At increasing cavity-magnetron duty cycle, they found that at approximately 30 kJ process energy budget they produced flower-like nanostructures and at an increased energy budget of 64 kJ they produced spherical nanostructures (green circle). Ngo et al. [56] and Ngo et al. [61] used $Na_3C_6H_5O_7$ in H_2O to reduce $HAuCl_4$ within an EMM1908W Electrolux microwave oven. At 210 W and an approximate process energy budget of 64 kJ and process energy density of 3.2 $kJ{\cdot}ml^{-1}$ that yielded spherical nanoparticles. Shah and Zheng [58] used (3-mercaptopropyl) trimethoxysilane ($HS(CH_2)_3Si(OCH_3)_3$) plus H_2O to reduce $HAuCl_4$ within a R202ZS Sharp microwave oven. At 800 W the process produced hexagonal Au nanostructures at an approximate process energy budget of 37.8 kJ and process energy density of 16 $kJ{\cdot}ml^{-1}$ (yellow filled circle, black ring). Putri et al. [60] used a one-pot synthesis of white bol guava leaf extract in ethanol to reduce $HAuCl_4$ within a NN-SM33HM/W Panasonic microwave oven at 800 W at an approximate process energy budget of 64.3 kJ and process energy density of 1.9 $kJ{\cdot}ml^{-1}$. Blosi et al. [37] used the Milstone SYNTH digestion applicator that employs two cavity-magnetrons to synthesis Au core bimetallic Au-Ag particles. In this 'Green' synthesis $HAuCl_4$ is reduced by $C_6H_{12}O_6$ in alkaline H_2O at T_B = 90 °C. The cavity-magnetron applied power was ramped-up and held at a T_B = 80 °C, as determined by software that controls the power level for 300 s. Finally, Marinoiu et al. [59] used an 'eco-friendly' one-step hydrothermal process (800 W, T_B = 60 to 80 °C) to synthesize Au nanostructures supported on a graphene oxide within a MARS-6 Digestion applicator (large yellow filled diamond with green outer edge). Finally out of these Pt and Au syntheses [37,53–57,59–61] may be placed in the recommended Green Chemistry group.

7.4. Compilation of transition metal synthesis

Figure 8 shows the microwave-assisted energy phase-space for the three chemistry groups along with four E-F_m calculated examples (large filed circles) as a guide a lower exponent = 0.66 and a upper exponent = 0.87 is used.

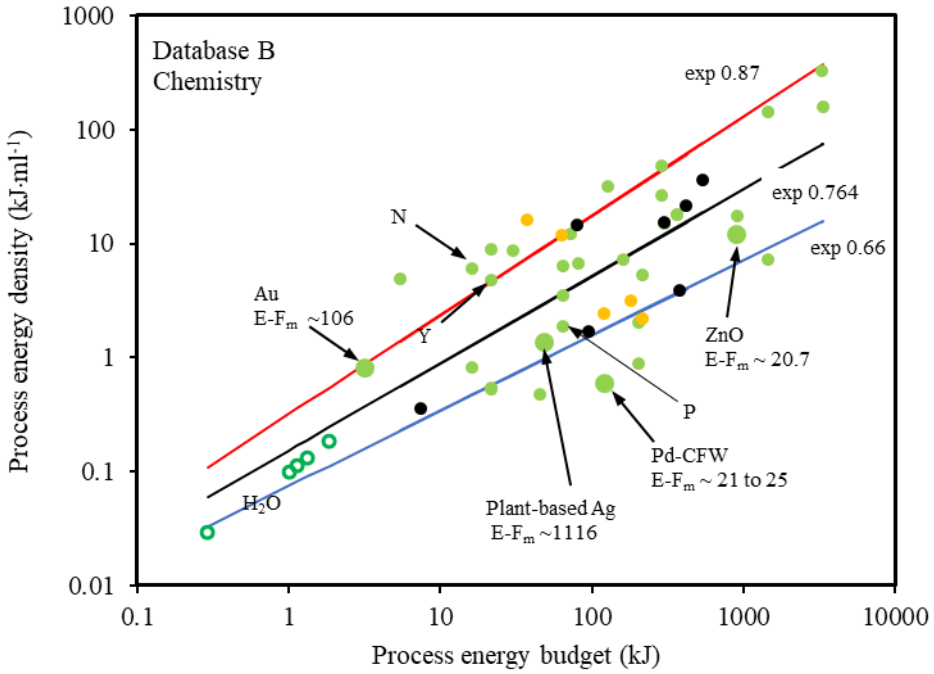

Figure 8. Log-log energy phase-space projection of Green Chemistry (green circles), problematic group (tan circles), non-Green Chemistry hazardous group (black circles). The open green circles = Microwave oven heating of water. Allometry scaling: red line = exponent 0.87, blue line = exponent 0.66, and black line = original trend-line with an exponent = 0.764. The annotated letters M, Y, and P correspond to Mallikarjuna and Varma [53], Yasmim et al. [54], and Purti et al. [60]. Reproduced and updated from Law and Dowling [8].

The first feature of note here is that the recommended Green Chemistry group ranges from the non-thermal-microwave heating studies at the bottom left to the hydrothermal and solvothemal synthesis in the upper right; with $C_6H_{12}O_6$, and $C_{12}H_{22}O_{11}$) [53], *hibiscus rosa-sinensis* leaf extract [54], and white bol guava leaf extract [60] in the mid energy range. The second feature is that the bacterial exopolysaccharide used to reduce $HAuCl_4$ to Au nanostructure is expected to be in this region; however, there is insufficient data to plot this synthesis [86].

The second feature of note is that the two exponents 0.66 and 0.87 bracket the non-Green Chemistry hazardous synthesis range over two orders of magnitude (10 to 100 kJ). In addition, the problematic Green Chemistry group exhibits a tight grouping between 37.5 and 200 kJ with the upper exponent close to 0.94 and the lower exponent close to 0.64, or 0.02 from the non-Green chemistry hazardous lower exponent.

The third feature of note is the four 50% metal yield E-F_m data points (large green circles) are located in the recommended Green Chemistry group bracketed by the exponent = 0.87 and exponent 0.57. Inspite of this the monometallic Ag and Au nanostructures are located in the 5 to 100 kJ regions, and the ZnO, and Pd supported on carbon framework are in the 100 to 1000 kJ regions. In contrast to the rank plot, the energy phase-space projection shows that E-F_m value decreases with increasing process energy budget there is discrimination between microwave applicator-type and reactants. In order to thoroughly understand this outlook further investigation is required.

8. Summary

This work has brought together four published articles on the subject of microwave-assisted synthesis of transition metal (monometallic, bimetallic, and metal supported on carbon framework) nanostructures [5–8]. The focus of the working is to study the underling dynamic of transition metal (Zn, Pd, Ag, Pt Au) processing data contained within Database B. It is implicit in this work that the microwave energy process is 'Green' with respect to traditional (thermal) process. But how 'Green' is one microwave process compared to another is investigated here. For this reason microwave applicator-type, metal precursor, reactant, solvent, target product, and waste are displayed in a log-log process energy phase projection. Fifty synthesized transition metals syntheses reported on, that yield a power-law signature of $y = 0.3293x^{0.846}$, $R^2 = 0.7923$ over four orders of magnitude.

Residual error analysis of the power-law signature is used to indentify outliers. Outlier found in the high process energy and energy zone of the energy phase-space projection are linked to microwave digestion type microwave application-type.

Mass-based E-F_m metrics has been used to evaluate the 'Greenness' of one-step (facile) microwave-assisted synthesis of solid spherical or oval-like monometallic ZnO, Ag and Au, and Pd supported on carbon framework nanostructures. For 50% metal yield, it is generally shown that the monometallic nanostructures have E-F_m values from 100 to 1000, where the upper value is determined by the amount of reducing reagent and solvent used: this being particularly true for plant-based synthesis. Palladium supported on carbon frameworks has a relatively low E-F_m value in the 10 s, due to the reactants are incorporated into the metal nanostructure product.

A dual allometry discrimination test has been developed. The main discrimination test outcomes are:

First transition metal period and row

'Green Chemistry' microwave-assisted synthesis of ZnO nanostructures exhibit a broad *y*-axes distribution within an allometry upper exponent = 0.9 and lower exponent = 0.57, the intercept of both boundaries are aligned to a power-law signature *y*-axes intercept 0.7837. Non-Green Chemistry microwave-assisted synthesis of ZnO nanostructures exhibit a narrower bandwidth between exponent = 0.764 and exponent = 0.57.

Second transition metal period and row

The Pt and Ag nanostructure synthesis fall within the upper boundary exponent = 1 and the lower exponent = 0.57. Only one data point is positioned at exponent = 1.

Third transition metal period and row

The majority (fifteen) of the Pd and Au nanostructure synthesis fall within the upper exponent = 0.95 and lower exponent = 0.764. Only one Au synthesis is below the original trend-line at an exponent = 0.7.

With regard to Recommended Green Chemistry test, the data (H_2O and $C_2H_4(OH)_2$) exhibits a broad *y*-axes distribution within an exponent = 1 and exponent = 0.5. Simple lightweight caustic chemicals (KOH, NaOH and Na_2O_2) are that are placed in the problematic Green Chemistry group exhibits a narrower distribution on the *y*-axes within an exponent = 0.94 and exponent = 0.64. And finally, Non-Green Chemistry hazardous solvent data (organic-bromide and flammable/toxic hydrazine

hydrate) exhibits a further narrowing of the *y*-axes distribution within the exponent = 0.87 and exponent = 0.66.

9. Outlook

The use of energy phase-space projection along with mass-based E-F_m metrics environment allometry discrimination test allows researchers to test their microwave-assisted synthesis in term of energy use and greenness. Both criteria are important in sustainable development in chemical processing. The metrics discussed in this works does not include the environmental impact of the generated waste. Where the generated waste contains non-consumed transition metal this is an environment concern and ways to incorporate an environmental metric needs further investigation.

Acknowledgments: This work was first presented as a plenary talk at the 17th Chaos International conference 11–14th June 2024, Cultural Center of Chania Crete, Greece. Dr Law would like to thank the conference committee for their support and encouragement of this work.

Conflict of interest: The authors declare no conflict of interest.

References

1. Mehta G, Krief A, Hopf H, et al. Chemistry in a post-Covid-19 world. AsiaChem Magazine. 2020; 1(1). doi: 10.51167/acm00013
2. Anastas PT, Farris CA. Benign by Design. ACS Symposium Series; 1994.
3. Anastas P, Eghbali N. Green Chemistry: Principles and Practice. Chem Soc Rev. 2010; 39(1): 301-312. doi: 10.1039/b918763b
4. Bharadwaj KK, Rabha B, Pati S, et al. Green Synthesis of Gold Nanoparticles Using Plant Extracts as Beneficial Prospect for Cancer Theranostics. Molecules. 2021; 26(21): 6389. doi: 10.3390/molecules26216389
5. Law VJ, Dowling DP. Revisiting "Non-Thermal" Batch Microwave Oven Inactivation of Microorganisms. American Journal of Analytical Chemistry. 2023; 14(01): 28-54. doi: 10.4236/ajac.2023.141003
6. Law VJ, Dowling DP. Microwave-Assisted Au and Ag Nanoparticle Synthesis: An Energy Phase-Space Projection Analysis. American Journal of Analytical Chemistry. 2023; 14(04): 149-174. doi: 10.4236/ajac.2023.144009
7. Law VJ, Dowling DP. Microwave-Assisted Transition Metal Nanostructure Synthesis: Power-Law Signature Verification. American Journal of Analytical Chemistry. 2023; 14(08): 326-349. doi: 10.4236/ajac.2023.148018
8. Law VJ, Dowling DP. Green Chemistry Allometry Test of Microwave-Assisted Synthesis of Transition Metal Nanostructures. American Journal of Analytical Chemistry. 2023; 14(11): 493-518. doi: 10.4236/ajac.2023.1411029
9. Andriani P, McKelvey B. Perspective—From Gaussian to Paretian Thinking: Causes and Implications of Power Laws in Organizations. Organization Science. 2009; 20(6): 1053-1071. doi: 10.1287/orsc.1090.0481
10. Stumpf MPH, Porter MA. Critical Truths About Power Laws. Science. 2012; 335(6069): 665-666. doi: 10.1126/science.1216142
11. Roman S, Bertolotti F. A master equation for power laws. Royal Society Open Science. 2022; 9(12). doi: 10.1098/rsos.220531
12. Hınıs M, Yeşildal TK, Erdönmez D, et al. Green Synthesis of Silver Nanoparticles from Sumac Extract by Microwave-Assisted and Traditional Method: Characterization, Anticancer and Antimicrobial Activities. Springer Science and Business Media LLC; 2024.
13. Sheldon RA. Metrics of Green Chemistry and Sustainability: Past, Present, and Future. ACS Sustainable Chemistry & Engineering. 2017; 6(1): 32-48. doi: 10.1021/acssuschemeng.7b03505
14. Bondarenko O, Juganson K, Ivask A, et al. Toxicity of Ag, CuO and ZnO nanoparticles to selected environmentally relevant test organisms and mammalian cells in vitro: a critical review. Archives of Toxicology. 2013; 87(7): 1181-1200. doi:

10.1007/s00204-013-1079-4
15. Liu S, Maljovec D, Wang B, et al. Visualizing High-Dimensional Data: Advances in the Past Decade. IEEE Transactions on Visualization and Computer Graphics. 2017; 23(3): 1249-1268. doi: 10.1109/tvcg.2016.2640960
16. Andresen B, Shiner JS, Uehlinger DE. Allometric scaling and maximum efficiency in physiological eigen time. Proceedings of the National Academy of Sciences. 2002; 99(9): 5822-5824. doi: 10.1073/pnas.082633699
17. Huxley JS, Teissier G. Terminology of Relative Growth. Nature. 1936; 137(3471): 780-781. doi: 10.1038/137780b0
18. Huxley JS, Teissier G. Terminologie et notation dans la description de la croissance relative. Comptes rendus des séances de la Société de biologie et de ses filiales. 1936; 121: 934-937.
19. Morsy SMI. Role of surfactants in nanotechnology and their applications. International Journal of Current. Microbiology and Applied Science. 2014; 3(5): 237-260.
20. Ballhausen CJ. Molecular electronic structures of transition metal complexes. McGraw-Hill International Book Company; 1979.
21. Murr LE. Handbook of Materials Structures, Properties, Processing and Performance. Springer Nature Link; 2015.
22. Cao J, Wang J, Fang B, et al. Microwave-assisted Synthesis of Flower-like ZnO Nanosheet Aggregates in a Room-temperature Ionic Liquid. Chemistry Letters. 2004; 33(10): 1332-1333. doi: 10.1246/cl.2004.1332
23. Li H, Liu E tao, Chan FYF, et al. Fabrication of ordered flower-like ZnO nanostructures by a microwave and ultrasonic combined technique and their enhanced photocatalytic activity. Materials Letters. 2011; 65(23-24): 3440-3443. doi: 10.1016/j.matlet.2011.07.049
24. Cao Y, Liu B, Huang R, et al. Flash synthesis of flower-like ZnO nanostructures by microwave-induced combustion process. Materials Letters. 2011; 65(2): 160-163. doi: 10.1016/j.matlet.2010.09.072
25. Li X, Wang C, Zhou X, et al. Gas sensing properties of flower-like ZnO prepared by a microwave-assisted technique. RSC Adv. 2014; 4(88): 47319-47324. doi: 10.1039/c4ra07425d
26. Hasanpoor M, Aliofkhazraei M, Delavari H. Microwave-assisted Synthesis of Zinc Oxide Nanoparticles. Procedia Materials Science. 2015; 11: 320-325. doi: 10.1016/j.mspro.2015.11.101
27. Krishnapriya R, Praneetha S, Murugan AV. Investigation of the effect of reaction parameters on the microwave-assisted hydrothermal synthesis of hierarchical jasmine-flower-like ZnO nanostructures for dye-sensitized solar cells. New Journal of Chemistry. 2016; 40(6): 5080-5089. doi: 10.1039/c6nj00457a
28. Wojnarowicz J, Opalinska A, Chudoba T, et al. Effect of Water Content in Ethylene Glycol Solvent on the Size of ZnO Nanoparticles Prepared Using Microwave Solvothermal Synthesis. Journal of Nanomaterials. 2016; 2016: 1-15. doi: 10.1155/2016/2789871
29. Wojnarowicz J, Chudoba T, Gierlotka S, et al. Size Control of Cobalt-Doped ZnO Nanoparticles Obtained in Microwave Solvothermal Synthesis. Crystals. 2018; 8(4): 179. doi: 10.3390/cryst8040179
30. Liu H, Liu H, Yang J, et al. Microwave-assisted one-pot synthesis of Ag decorated flower-like ZnO composites photocatalysts for dye degradation and NO removal. Ceramics International. 2019; 45(16): 20133-20140. doi: 10.1016/j.ceramint.2019.06.279
31. Aljaafari A, Ahmed F, Awada C, et al. Flower-Like ZnO Nanorods Synthesized by Microwave-Assisted One-Pot Method for Detecting Reducing Gases: Structural Properties and Sensing Reversibility. Frontiers in Chemistry. 2020; 8. doi: 10.3389/fchem.2020.00456
32. Cai Y, Huang J. Preparation and Photocatalysis Characteristics of Flower-like ZnO by Microwave Method. Journal of Physics: Conference Series. 2023; 2437(1): 012039. doi: 10.1088/1742-6596/2437/1/012039
33. Elazab HA, Moussa S, Gupton BF, et al. Microwave-assisted synthesis of Pd nanoparticles supported on Fe_3O_4, Co_3O_4, and Ni(OH)2 nanoplates and catalysis application for CO oxidation. Journal of Nanoparticle Research. 2014; 16(7). doi: 10.1007/s11051-014-2477-0
34. Elazab HA, Sadek MA, El-Idreesy TT. Microwave-assisted synthesis of palladium nanoparticles supported on copper oxide in aqueous medium as an efficient catalyst for Suzuki cross-coupling reaction. Adsorption Science & Technology. 2018; 36(5-6): 1352-1365. doi: 10.1177/0263617418771777
35. Rademacher L, Beglau THY, Heinen T, et al. Microwave-assisted synthesis of iridium oxide and palladium nanoparticles supported on a nitrogen-rich covalent triazine framework as superior electrocatalysts for the hydrogen evolution and oxygen reduction reaction. Frontiers in Chemistry. 2022; 10. doi: 10.3389/fchem.2022.945261
36. Chen J, Wang J, Zhang X, et al. Microwave-assisted green synthesis of silver nanoparticles by carboxymethyl cellulose

sodium and silver nitrate. Materials Chemistry and Physics. 2008; 108(2-3): 421-424. doi: 10.1016/j.matchemphys.2007.10.019

37. Blosi M, Albonetti S, Gatti F, et al. Au, Ag and Au-Ag nanoparticles: microwave-assisted synthesis in water and applications in ceramic and catalysis. Nanotech. 2010; 1: 352-355.
38. Saha S, Malik MM, Qureshi MS. Microwave Synthesis of Silver Nanoparticles. Nano Hybrids. 2013; 4: 99-112. doi: 10.4028/www.scientific.net/nh.4.99
39. Iqbal N, Abdul Kadir MR, Nik Malek NAN, et al. Characterization and antibacterial properties of stable silver substituted hydroxyapatite nanoparticles synthesized through surfactant assisted microwave process. Materials Research Bulletin. 2013; 48(9): 3172-3177. doi: 10.1016/j.materresbull.2013.04.068
40. Pal J, Deb MK, Deshmukh DK. Microwave-assisted synthesis of silver nanoparticles using benzo-18-crown-6 as reducing and stabilizing agent. Applied Nanoscience. 2013; 4(4): 507-510. doi: 10.1007/s13204-013-0229-6
41. Rai P, Majhi SM, Yu YT, et al. Synthesis of plasmonic Ag@SnO2 core–shell nanoreactors for xylene detection. RSC Advances. 2015; 5(23): 17653-17659. doi: 10.1039/c4ra13971b
42. Karimipour M, Mollaei M, Shabani E, et al. Microwave synthesis of Oleylamine -capped Ag nanoparticles in aqueous solution. Materials Science. 2015; 21(2). doi: 10.5755/j01.ms.21.2.6480
43. Ebrahimi M, Zakery A, Karimipour M, et al. Nonlinear optical properties and optical limiting measurements of graphene oxide – Ag@TiO2 compounds. Optical Materials. 2016; 57: 146-152. doi: 10.1016/j.optmat.2016.04.039
44. Karimipour M, Mostoufirad S, Molaei M, et al. Free reducing agent, one pot, and two steps synthesis of Ag@SiO2 core-shells using microwave irradiation. Journal of Nano- And Electronic Physics. 2016; 8(3).
45. Miglietta ML, Alfano B, Polichetti T, et al. Effective tuning of silver decorated graphene sensing properties by adjusting the Ag NPs coverage density. Springer International Publishing; 2018.
46. Jyothi D, Cheriyan SP, Ahmed SRR, et al. TG. Microwave assisted green synthesis of silver nanoparticles using coleus amboinicus leaf extract. International Journal of Applied Pharmaceutics; 2020.
47. Ahmed F, AlOmar SY, Albalawi F, et al. Microwave Mediated Fast Synthesis of Silver Nanoparticles and Investigation of Their Antibacterial Activities for Gram-Positive and Gram-Negative Microorganisms. Crystals. 2021; 11(6): 666. doi: 10.3390/cryst11060666
48. Li D, Komarneni S. Synthesis of Pt Nanoparticles and Nanorods by Microwave-assisted Solvothermal Technique. Zeitschrift für Naturforschung B. 2006; 61(12): 1566-1572. doi: 10.1515/znb-2006-1214
49. Kundu P, Nethravathi C, Deshpande PA, et al. Ultrafast Microwave-Assisted Route to Surfactant-Free Ultrafine Pt Nanoparticles on Graphene: Synergistic Co-reduction Mechanism and High Catalytic Activity. Chemistry of Materials. 2011; 23(11): 2772-2780. doi: 10.1021/cm200329a
50. Pal J, Deb MK, Deshmukh DK, et al. Microwave-assisted synthesis of platinum nanoparticles and their catalytic degradation of methyl violet in aqueous solution. Applied Nanoscience. 2012; 4(1): 61-65. doi: 10.1007/s13204-012-0170-0
51. Wojnicki M, Luty-Błocho M, Kwolek P, et al. The influence of dielectric permittivity of water on the shape of PtNPs synthesized in high-pressure high-temperature microwave reactor. Scientific Reports. 2021; 11(1). doi: 10.1038/s41598-021-84388-2
52. Liu FK, Huang PW, Chang YC, et al. Formation of silver nanorods by microwave heating in the presence of gold seeds. Journal of Crystal Growth. 2005; 273(3-4): 439-445. doi: 10.1016/j.jcrysgro.2004.09.043
53. Mallikarjuna NN, Varma RS. Microwave-assisted shape-controlled bulk synthesis of noble nanocrystals and their catalytic properties. Crystal Growth & Design. 2007; 7(4): 686-690.
54. Yasmin A, Ramesh K, Rajeshkumar S. Optimization and stabilization of gold nanoparticles by using herbal plant extract with microwave heating. Nano Convergence. 2014; 1(1). doi: 10.1186/s40580-014-0012-8
55. Bhosale MA, Chenna DR, Ahire JP, et al. Morphological study of microwave-assisted facile synthesis of gold nanoflowers/nanoparticles in aqueous medium and their catalytic application for reduction of p-nitrophenol to p-aminophenol. RSC Advances. 2015; 5(65): 52817-52823. doi: 10.1039/c5ra05731k
56. Ngo VKT, Nguyen HPU, Huynh TP, et al. Preparation of gold nanoparticles by microwave heating and application of spectroscopy to study conjugate of gold nanoparticles with antibody E. coli O157: H7. Advances in Natural Sciences: Nanoscience and Nanotechnology. 2015; 6(3): 035015. doi: 10.1088/2043-6262/6/3/035015
57. Bayazit MK, Yue J, Cao E, et al. Controllable Synthesis of Gold Nanoparticles in Aqueous Solution by Microwave Assisted Flow Chemistry. ACS Sustainable Chemistry & Engineering. 2016; 4(12): 6435-6442. doi: 10.1021/acssuschemeng.6b01149

58. Shah KW, Zheng L. Microwave-assisted Synthesis of Hexagonal Gold Nanoparticles Reduced by Organosilane (3-Mercaptopropyl) trimethoxysilane. Materials. 2019; 12(10): 1680. doi: 10.3390/ma12101680
59. Marinoiu A, Andrei R, Vagner I, et al. One Step Synthesis of Au Nanoparticles Supported on Graphene Oxide Using an Eco-Friendly Microwave-Assisted Process. Materials Science. 2020; 26(3): 249-254. doi: 10.5755/j01.ms.26.3.21857
60. Putri SE, Pratiwi DE, Side S. The Effect Of Microwave Irradiation on Synthesis of Gold Nanoparticles Using Ethanol Extract of White Bol Guava Leaves. Journal of Physics: Conference Series. 2021; 1752(1): 012058. doi: 10.1088/1742-6596/1752/1/012058
61. Ngo VKT, Nguyen DG, Huynh TP, et al. A low cost technique for synthesis of gold nanoparticles using microwave heating and its application in signal amplification for detecting Escherichia Coli O157: H7 bacteria. Advances in Natural Sciences: Nanoscience and Nanotechnology. 2016; 7(3): 035016. doi: 10.1088/2043-6262/7/3/035016
62. Kianpour M, Akbarian M, Uversky VN. Nanoparticles for Coronavirus Control. Nanomaterials. 2022; 12(9): 1602. doi: 10.3390/nano12091602
63. Kunal P, Toops TJ. A Review of Microwave-Assisted Synthesis-Based Approaches to Reduce Pd-Content in Catalysts. Catalysts. 2020; 10(9): 991. doi: 10.3390/catal10090991
64. Joudeh N, Linke D. Nanoparticle classification, physicochemical properties, characterization, and applications: a comprehensive review for biologists. Journal of Nanobiotechnology. 2022; 20(1). doi: 10.1186/s12951-022-01477-8
65. Baranov AN, Sokolov PS, Solozhenko VL. ZnO under Pressure: From Nanoparticles to Single Crystals. Crystals. 2022; 12(5): 744. doi: 10.3390/cryst12050744
66. Teterycz H, Rac O, Suchorska-Woźnaik P, et al. The formation mechanism of colloidal spheres of ZnO in ethylene glycol. Digest Journal of Nanomaterials and Biostructures. 2013; 8(3): 1157-1167.
67. Yang F, Gong J, Yang E, et al. Microwave-absorbing properties of room-temperature ionic liquids. Journal of Physics D: Applied Physics. 2019; 52(15): 155302. doi: 10.1088/1361-6463/ab016c
68. Kustov L, Vikanova K. Synthesis of Metal Nanoparticles under Microwave Irradiation: Get Much with Less Energy. Metals. 2023; 13(10): 1714. doi: 10.3390/met13101714
69. Law VJ, Dowling DP. Application of microwave oven plasma reactors for the formation of carbon-based nanomaterials. In: Skiadas C, Diomtiakis Y (editors). 13th Chaotic Modeling and Simulation International Conference. Springer, Berlin; 2021. pp. 467-486.
70. Kawasaki H. Surfactant-free solution-based synthesis of metallic nanoparticles toward efficient use of the nanoparticles' surfaces and their application in catalysis and chemo-/biosensing. Nanotechnology Reviews. 2013; 2(1): 5-25. doi: 10.1515/ntrev-2012-0079
71. Rana KK, Rana S. Microwave Reactors: A Brief Review on Its Fundamental Aspects and Applications. OALib. 2014; 01(06): 1-20. doi: 10.4236/oalib.1100686
72. Patil NG, Rebrov EV, Eranen K, et al. Effect of the Load Size on the Efficiency of Microwave Heating Under Stop Flow and Continuous Flow Conditions. Journal of Microwave Power and Electromagnetic Energy. 2012; 46(2): 83-92. doi: 10.1080/08327823.2012.11689827
73. Law VJ, Dowling DP. Microwave generated steam decontamination of respirators: dielectric considerations. GJRECS. 2021; 1(2): 6-2.
74. Welton T. Solvents and sustainable chemistry. Proceedings of the Royal Society A: Mathematical, Physical and Engineering Sciences. 2015; 471(2183): 20150502. doi: 10.1098/rspa.2015.0502
75. Gaba M, Dhingra N. Microwave chemistry: general features and applications. Indian Journal of Pharmaceutical Education and Research. 2011; 45(2): 175 – 182.
76. Harpeness R, Gedanken A. Microwave Synthesis of Core−Shell Gold/Palladium Bimetallic Nanoparticles. Langmuir. 2004; 20(8): 3431-3434. doi: 10.1021/la035978z
77. Abdelsayed V, Aljarash A, El-Shall MS, et al. Microwave Synthesis of Bimetallic Nanoalloys and CO Oxidation on Ceria-Supported Nanoalloys. Chemistry of Materials. 2009; 21(13): 2825-2834. doi: 10.1021/cm9004486
78. Siamaki AR, Khder AERS, Abdelsayed V, et al. Microwave-assisted synthesis of palladium nanoparticles supported on graphene: A highly active and recyclable catalyst for carbon–carbon cross-coupling reactions. Journal of Catalysis. 2011; 279(1): 1-11. doi: 10.1016/j.jcat.2010.12.003
79. Rai P, Kim SG, Yu YT. Microwave assisted synthesis of flower-like ZnO and effect of annealing atmosphere on its photoluminescence property. Journal of Materials Science: Materials in Electronics. 2011; 23(2): 344-348. doi:

10.1007/s10854-011-0384-z
80. Prakash T, Jayaprakash R, Neri G, et al. Synthesis of ZnO Nanostructures by Microwave Irradiation Using Albumen as a Template. Journal of Nanoparticles. 2013; 2013: 1-8. doi: 10.1155/2013/274894
81. Zhang J, Bai X. Microwave-Assisted Synthesis of Pd Nanoparticles and Catalysis Application for Suzuki Coupling Reactions. The Open Materials Science Journal. 2017; 11(1): 1-8. doi: 10.2174/1874088x01711010001
82. Gomez-Bolivar J, Mikheenko IP, Macaskie LE, et al. Characterization of Palladium Nanoparticles Produced by Healthy and Microwave-Injured Cells of Desulfovibrio desulfuricans and Escherichia coli. Nanomaterials. 2019; 9(6): 857. doi: 10.3390/nano9060857
83. Nishida Y, Wada Y, Chaudhari C, et al. Preparation of Noble-metal Nanoparticles by Microwave-assisted Chemical Reduction and Evaluation as Catalysts for Nitrile Hydrogenation under Ambient Conditions. Journal of the Japan Petroleum Institute. 2019; 62(5): 220-227. doi: 10.1627/jpi.62.220
84. Yalcin M. Microwave-assisted synthesis of ZnO nanoflakes: structural, optical and dielectric characterization. Materials Research Express. 2020; 7(5): 055019. doi: 10.1088/2053-1591/ab940f
85. Jaimes-Paez CD, Vences-Alvarez E, Salinas-Torres D, et al. Microwave-assisted synthesis of carbon-supported Pt nanoparticles for their use as electrocatalysts in the oxygen reduction reaction and hydrogen evolution reaction. Electrochimica Acta. 2023; 464: 142871. doi: 10.1016/j.electacta.2023.142871
86. El-Naggar ME, Shaheen TI, Fouda MMG, et al. Eco-friendly microwave-assisted green and rapid synthesis of well-stabilized gold and core–shell silver–gold nanoparticles. Carbohydrate Polymers. 2016; 136: 1128-1136. doi: 10.1016/j.carbpol.2015.10.003
87. Lindstedt SL, Calder, WA. Body Size, Physiological Time, and Longevity of Homeothermic Animals. The Quarterly Review of Biology. 1981; 56(1): 1-16. doi: 10.1086/412080
88. Law VJ. Microwave near-field plasma probe. Vacuum. 1998; 51(3): 463-468. doi:10.1016/S0042-207X(98)00199-7
89. Geedipalli SSR, Rakesh V, Datta AK. Modeling the heating uniformity contributed by a rotating turntable in microwave ovens. Journal of Food Engineering. 2007; 82(3): 359-368. doi: 10.1016/j.jfoodeng.2007.02.050
90. Dong H, Li M, Liu R, et al. Allometric scaling in scientific fields. Scientometrics. 2017; 112(1): 583-594. doi: 10.1007/s11192-017-2333-y
91. Kleiber M. Body size and metabolism. Hilgardia. 1932; 6(11): 315-353. doi: 10.3733/hilg.v06n11p315
92. Kleiber M. Body size and metabolic rate. Physiological Reviews. 1947; 27(4): 511-541. doi: 10.1152/physrev.1947.27.4.511
93. Gillooly JF, Brown JH, West GB, et al. Effects of Size and Temperature on Metabolic Rate. Science. 2001; 293(5538): 2248-2251. doi: 10.1126/science.1061967
94. Downs CJ, Hayes JP, Tracy CR. Scaling metabolic rate with body mass and inverse body temperature: a test of the Arrhenius fractal supply model. Functional Ecology. 2007; 22(2): 239-244. doi: 10.1111/j.1365-2435.2007.01371.x
95. Rau ARP. Biological scaling and physics. Journal of Biosciences. 2002; 27(5): 475-478. doi: 10.1007/bf02705043
96. Agutter PS, Tuszynski JA. Analytic theories of allometric scaling. Journal of Experimental Biology. 2011; 214(7): 1055-1062. doi: 10.1242/jeb.054502
97. Niklas KJ, Kutschera U. Kleiber's Law: How theFire of Lifeignited debate, fueled theory, and neglected plants as model organisms. Plant Signaling & Behavior. 2015; 10(7): e1036216. doi: 10.1080/15592324.2015.1036216
98. Lamont BB, Williams MR, He T. Relative growth rate (RGR) and other confounded variables: mathematical problems and biological solutions. Annals of Botany. 2023; 131(4): 555-568. doi: 10.1093/aob/mcad031
99. Alfano B, Polichetti T, Mauriello M, et al. Modulating the sensing properties of graphene through an eco-friendly metal-decoration process. Sensors and Actuators B: Chemical. 2016; 222: 1032-1042. doi: 10.1016/j.snb.2015.09.008
100. Min GI, Han SJ, Shin DM. Inverter circuit of microwave oven. US Patent 6936803B2; 2005.